SCIENTIFIC REPORTS

OPEN

SUBJECT AREAS:
SEMICONDUCTORS
OPTICAL PROPERTIES AND DEVICES
APPLIED PHYSICS
MECHANICAL AND STRUCTURAL PROPERTIES AND DEVICES

Received
12 September 2012

Accepted
16 January 2013

Published
1 February 2013

Correspondence and requests for materials should be addressed to T.Y. (yuting@ntu.edu.sg)

Visualization of arrangements of carbon atoms in graphene layers by Raman mapping and atomic-resolution TEM

Chunxiao Cong[1], Kun Li[2], Xi Xiang Zhang[2] & Ting Yu[1,3,4]

[1]Division of Physics and Applied Physics, School of Physical and Mathematical Sciences, Nanyang Technological University, Singapore 637371, (Singapore), [2]Advanced Nanofabrication, Imaging and Characterization Core Lab, King Abdullah University of Science and Technology (KAUST), Thuwal 239955, Kingdom of Saudi Arabia, [3]Department of Physics, Faculty of Science, National University of Singapore, Singapore 117542, (Singapore), [4]Graphene Research Centre, National University of Singapore, Singapore 117546, (Singapore).

In-plane and out-of-plane arrangements of carbon atoms in graphene layers play critical roles in the fundamental physics and practical applications of these novel two-dimensional materials. Here, we report initial results on the edge/crystal orientations and stacking orders of bi- and tri-layer graphene (BLG and TLG) from Raman spectroscopy and transmission electron microscopy (TEM) experiments performed on the same sample. We introduce a new method of transferring graphene flakes onto a normal TEM grid. Using this novel method, we probed the BLG and TLG flakes that had been previously investigated by Raman scattering with high-resolution (atomic) TEM.

The electronic band structures and physical properties of graphene layers depend on the in-plane and out-of-plane arrangement of their carbon atoms, which are reflected in their edge/crystal orientations and stacking orders, respectively. The influence of the edge orientation on the physical properties of graphene flakes and nanoribbons has been predicted theoretically and measured experimentally[1–10]. Recently, the stacking sequence of graphene layers, that is, the out-of-plane arrangement of the carbon atoms, has been the focus of research. For example, many interesting and important physical properties have been discovered in ABC-stacked trilayer graphene[11–17].

Several techniques, such as atomic force microscopy (AFM), scanning tunneling microscopy (STM), transmission electron microscopy (TEM) and Raman spectroscopy, have been used to study the edge/crystal orientations and the stacking orders of graphene[18–30]. Among them, Raman spectroscopy with Raman mapping is the most favored due to its high spectral efficiency (tens of milliseconds integration time for a clear spectrum), non-destructiveness and lack of special sample preparation. In addition to identifying the arrangements of carbon atoms in graphene, Raman spectroscopy is also able to determine the number of layers[31,32], the electronic structure[33–35], electron-phonon interactions[36-38], phonon dispersion relations[39], doping levels[40–42], defects[43,44], and strains[45–48]. Although Raman spectroscopy has been widely adopted in graphene research, its intrinsic spatial resolution of microns limits the direct visualization of the carbon atoms on an atomic scale. Thus, high-resolution AFM, TEM and STM are also useful. It is now possible to resolve every single carbon atom by HRTEM with the development of the aberration-corrected, monochromated TEM microscope[20,49,50].

Graphene flakes are usually prepared by mechanical exfoliation of natural graphite crystals or highly oriented pyrolytic graphite (HOPG) on a silicon substrate with a 300 nm silicon dioxide layer (SiO_2/Si)[51]. To perform TEM experiments on graphene flakes on SiO_2/Si substrates, it is necessary to transfer pre-selected graphene flakes onto a TEM grid. Thus far, only a few efficient methods to transfer grapheme flakes have been proposed. The best one, so far, promises about a 25% success rate using a very expensive and specially fabricated TEM grid[52].

In this work, we report on the identification of the in-plane and out-of-plane arrangements of carbon atom layers (bi- and tri-layers) by Raman spectroscopy and high-resolution TEM characterization. With a simple, one-step pre-treatment of the SiO_2/Si substrate by O_2 plasma, we improved the existing method for transferring graphene flakes and gain a success rate of 70%. Furthermore, we used a normal rather than a specially fabricated TEM grid. Thus, for the first time, we were able to study bi- and tri-layer graphene (BLG and TLG) flakes by Raman spectroscopy and then transfer them onto a normal TEM Cu grid for TEM study. As in our earlier observations of single-layer graphene (SLG), the dominant edge orientations and the crystal orientations of BLG

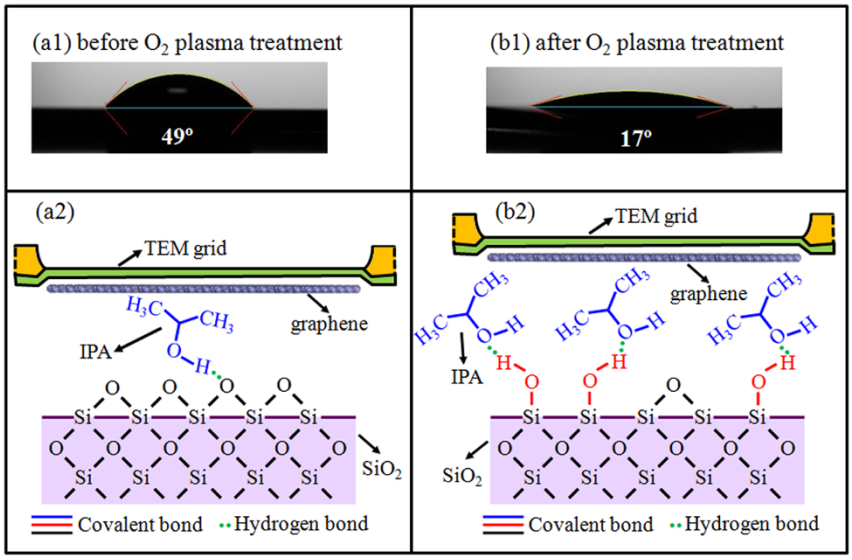

Figure 1 | Optical images of a water droplet on the SiO_2/Si substrate before (a1) and after (b1) O_2 plasma treatment. (a2) and (b2) present schematic diagrams of the transfer of graphene flakes onto a TEM grid from SiO_2/Si substrates without and with O_2 plasma treatment, respectively.

and TLG could be determined by monitoring the D band intensity[21] and G band position[24]. In addition, we were able to use TEM to visualize the arrangements of the carbon atoms at the atomic level to substantiate our Raman results.

Results

Figure 1 shows our modified transfer process. The key step that guarantees a high success rate and relaxes the requirement of a C-flat TEM grid is treatment of the SiO_2/Si substrate with O_2 plasma. As can be seen in Figures 1(a1) and 1(b1), the hydrophilicity of the surface of the SiO_2/Si substrate increased with O_2 plasma treatment, as indicated by the change in the contact angle from 49° to 17°. This is mainly due to the modification of the surface structures of the siloxane groups (Si-O-Si) in the as-purchased SiO_2/Si substrate to silanol groups (Si-OH) in the O_2 plasma-treated SiO_2/Si substrate. Immediately after the O_2 plasma process, the graphene flakes were mechanically exfoliated onto the pre-treated SiO_2/Si substrates[51]. These flakes, identified by optical microscopy and Raman spectroscopy, were then carefully covered by a normal TEM grid. We added a small drop of isopropanol alcohol (IPA) on top of the grid, which instantly spread out across the entire surface including the areas underneath graphene flakes because the silanol groups populate the surface of the O_2 plasma-treated SiO_2/Si substrate and attract the IPA molecules through hydrogen bonding. Thus, the superhydrophobic graphene flakes were lifted up and came into contact with the carbon film of the grid. The contact between the graphene flakes and carbon film of the grid was strengthened by the surface tension during the full evaporation of the IPA through illumination with a small incandescent lamp. To lift up the grid with the graphene flakes, we dropped a second droplet of IPA next to the grid. After the grid was then picked up and dried carefully in air, the suspended graphene flakes were ready for further investigation with TEM and Raman spectroscopy after some necessary cleaning processes.

The transfer of a TLG flake mechanically exfoliated from natural graphite crystals is shown in Figure 2. The graphene flake on the O_2 plasma-treated SiO_2/Si substrate was located by an optical microscope and further probed by Raman spectroscopy and mapping. After the first drop of IPA, the flake had the same contrast as the as-exfoliated flake (Figure 2(b)). As shown in Figure 2(c), the color of the flake changed from blue to gray after the second drop of IPA. This color change is a sign of success: the graphene flake had fully detached from the substrate and had become strongly anchored to the carbon film of the grid. Figure 2(d) shows a low-magnification TEM image and Raman images of the graphene flake after transfer onto the TEM grid.

Optical images recording the transfer of a BLG flake exfoliated from natural graphite crystals are presented in the Supporting Information (SI; Figure S1). Optical images of recording the transfer of graphene sheets with different numbers of layers exfoliated from HOPG are shown in Figure S2.

As previously described[21], we are interested in graphene flakes that have an angle of $(2n + 1) \times 30$ degrees (where n is an integer between 0 and 5) between two adjacent edges. In such flakes, it is highly likely that one edge is dominated by zigzag orientation while

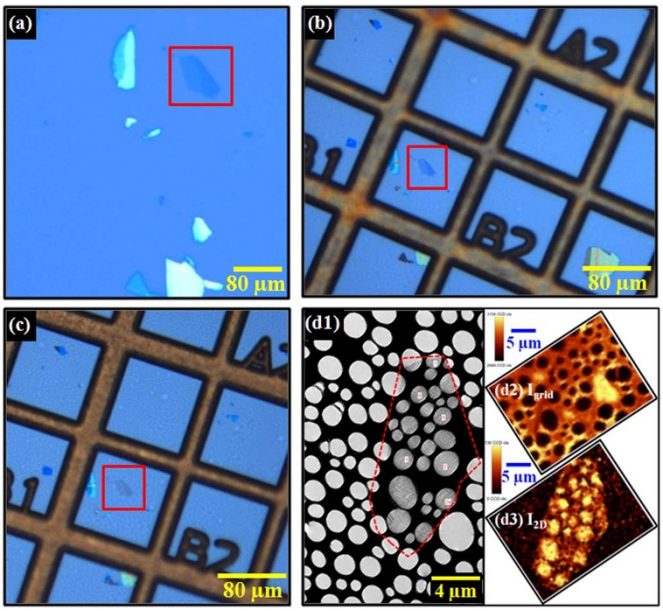

Figure 2 | Optical images of (a) a graphene flake on the O_2 plasma-treated SiO_2/Si substrate, (b) the graphene flake covered with a normal TEM grid after the first drop of IPA, (c) after the second of IPA. (d1) and (d3) show the TEM and Raman images of the same graphene flake on the TEM grid. (d2) shows the Raman image of the carbon film supporting the graphene flake.

the other is dominated by armchair orientation or vice versa. A BLG flake with a right angle corner is shown in Figure 3(a). The lineshape and width of the G′ (2D) peak indicate that this flake is a Bernal-stacked BLG. The Raman spectra of the two edges indicate a remarkable difference in the defect (D) and G modes, particularly the integrated intensity of the D mode and the position of the G mode in relation to one edge and the other. We used Raman mapping to clarify details about the entire region, especially the two edges, with the polarization of the incident laser 45 degrees to each edge, which ensured that the polarization effect influenced the two edges equally[25,26]. Figures 3(b) and 3(c) show the Raman images extracted from the D mode integrated intensity and the G mode position, respectively. As observed in SLG[21], one edge is bright, indicating an armchair orientation, while the other is relatively dark, suggesting its zigzag orientation. The obvious contrast of the D mode intensities from zigzag and armchair orientations could be understood by intervalley double resonant scattering[53]. Compared to the SLG[21], the contrast of BLG is not remarkable, at least in this flake, which might be due to the lower chance of having a neat edge in thick layers prepared by mechanical exfoliation. The Raman modes selection rule and the Kohn anomaly result in a difference in the G mode positions in zigzag- and armchair-dominated edges[23,24], which agrees with the identification by the D mode intensity.

To study the crystal structure of this BLG flake at the atomic level, we transferred the same sample to a normal TEM Cu grid. Figure 4(a) shows a typical low-magnification TEM image of the BLG flake together with that of a TLG flake. The schematic diagram of the edge/crystal orientation of the BLG, identified by our Raman study, is presented in the optical image in Figure 4(b), where the two flakes are oriented along the same direction in the TEM image. Although the most interesting corner (as indicated by Raman mapping in Figure 3) was scrolled during transfer process, the entire BLG flake should share the same crystal orientation because it was prepared by peeling it off from natural single crystalline graphite. In fact, our

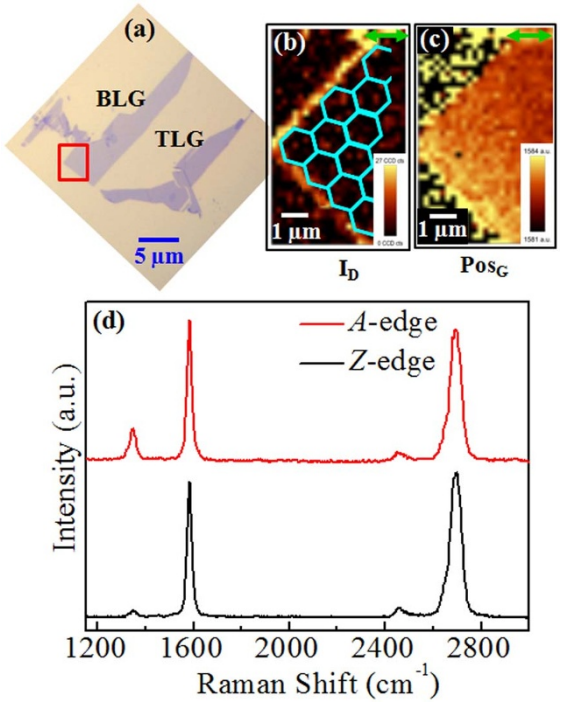

Figure 3 | (a) An optical image of BLG and TLG. The right-angle corner of BLG is highlighted. (b) A Raman D band integrated intensity image and (c) the Raman G band position of the highlighted area. The green arrows indicate the polarization of the incident laser. (d) Typical Raman spectra of the zigzag and armchair edges of BLG.

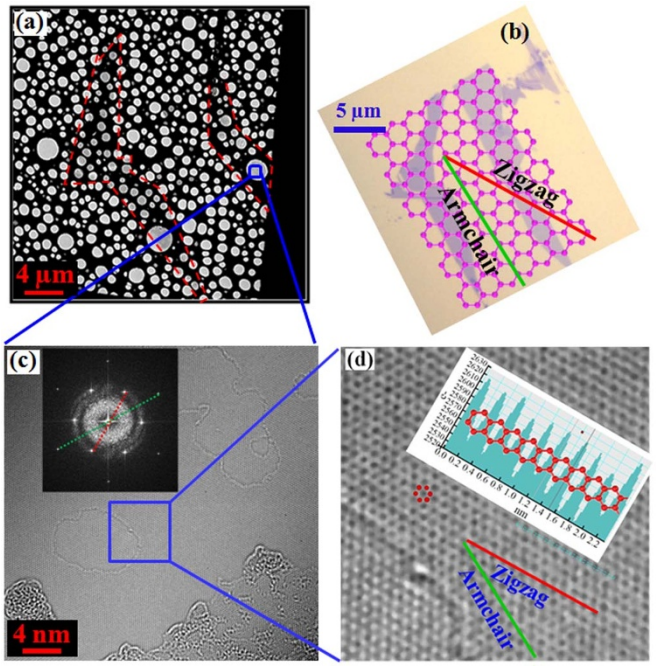

Figure 4 | (a) A TEM image of the BLG and TLG flakes after being transferred onto a normal TEM Cu grid. (b) An optical image of the BLG and TLG with the schematic diagram of the crystal orientation determined by Raman spectroscopy. The green and red lines indicate the armchair and zigzag directions, respectively. (c) An HRTEM image of the BLG. The inset of (c) is FFT of (c). The red line connecting the symmetrical pair of dots on the inner circle (corresponding to 0.213 nm spacing) is perpendicular to the zigzag direction of the graphene layers, while the green line connecting the symmetrical pairs of dots on the outer circle (corresponding to 0.123 nm spacing) is perpendicular to the armchair direction of the graphene layers. (d) An atomic-level HRTEM image of the BLG. The inset of (d) shows the line intensity profile of the light blue dotted line. The obtained readings perfectly match the lattice spacing of graphene.

HRTEM study indicates that the TLG has the same crystal orientation (not shown here). Figure 4(c) presents an HRTEM image of the BLG without a filter. Although we controlled the voltage during our TEM measurements to as low as 60 kV, obvious damage, such as "kicking off" the top layer by the e-beam, can be clearly seen. The damage rate is reduced in this image as compared with images made at higher kV. Inset of Figure 4(c) is the fast Fourier transform (FFT) of the HRTEM image of Figure 4(c). The peak positions of the FFT at different spatial frequencies show the armchair and zigzag orientations of the graphene layers. As shown in the inset of Figure 4(c), the red line connecting the symmetrical pair of dots on the inner circle (corresponding to 0.213 nm spacing) is perpendicular to the zigzag direction of the graphene layers, while the green line connecting the symmetrical pairs of dots on the outer circle (corresponding to 0.123 nm spacing) is perpendicular to the armchair direction of the graphene layers. Figure 4(d) shows an enlargement of Figure 4(c). In Figure 4(d), the zigzag and armchair orientations are clearly identified and labeled. They perfectly match the orientations determined in our Raman measurements shown in Figure 4(b). The line intensity profile (inset of Figure 4(d)) further confirms our identification of the zigzag orientation. In the inset of Figure 4 (d), the distance between the two peaks in the line intensity profile is ~0.25 nm, which is very close to the distance between the two next-nearest carbon atoms along the zigzag orientation of 0.246 nm. Thus, we present the first atomic-level HRTEM evidence of the edge/crystal orientation of BLG.

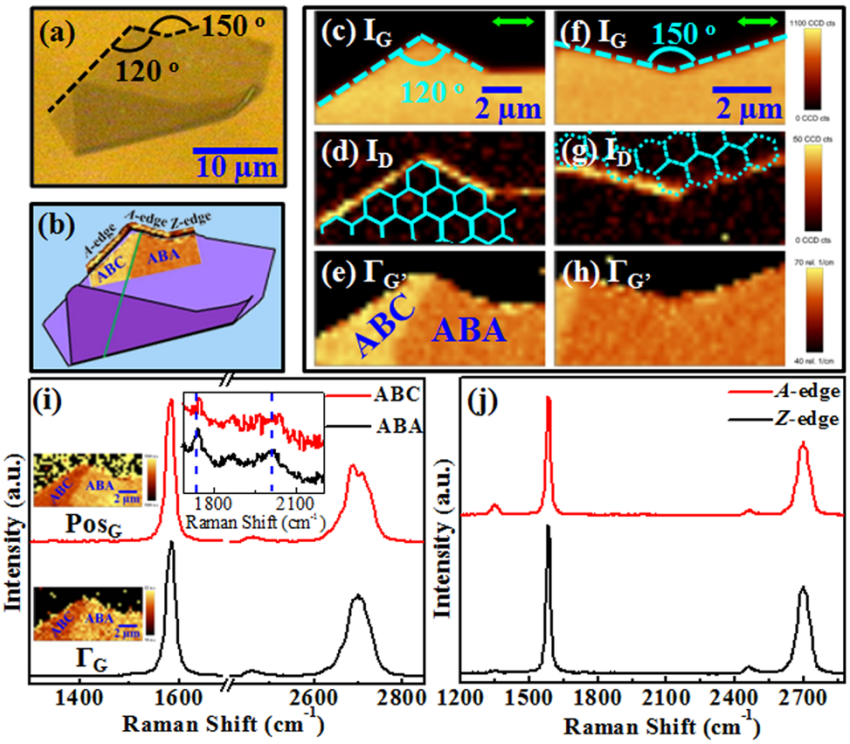

Figure 5 | (a) An optical image of TLG. (b) A schematic diagram of the TLG. The inset image indicates the edge orientations and stacking orders. (c, f) and (d, g) are Raman images of the G mode and D mode integrated intensity, respectively. The cartoons illustrate the edge/crystal orientations determined by the Raman mapping. (e, h) Raman images of the G′ mode width. (i) Typical Raman spectra of ABA- and ABC-stacked TLG domains. The inset images show the Raman mapping of the G mode positions and widths for the TLG of two types of stacked domains. The inset spectra show the modes in the intermediate frequency range. The relative shifts of the combinational modes are the spectral natures of these two types of TLG[29].

Figure 5 shows an optical image and Raman investigations of TLG. In addition to the in-plane arrangement, TLG has interesting out-of-plane arrangements, its so-called stacking order. It can be seen from the optical image of the graphene sample shown in Figure 5(a) that there are angles of 120 and 150 (or 210) degrees between two adjacent edges. The homogeneous contrast of the Raman images of the G band intensity shown in Figures 5(c) and 5(f) clearly indicates that the sample thickness or the number of graphene layers is the same over the entire sheet except for the folded part at the bottom. The white light contrast spectrum (not shown here) and the Raman spectra (Figures 5(i) and 5(j)) indicate that this is a TLG flake except for the folded part. The detailed Raman mapping of the D mode (Figures 5(d) and 5(g)) reveals that the two edges of the 120 degree angle are dominated by the armchair orientation while the other edge of the 150 degree is dominated by the zigzag orientation. To determine the stacking order, we plotted the Raman images of the G′ mode width in Figures 5(e) and 5(h). The broader linewidth of the G′ mode in the ABC-stacked TLG is the consequence of its unique electronic band structures, especially at the low energy level, and of the strong electron-phonon coupling in graphene as discussed previously[29]. The other spectral differences between ABA- and ABC-stacked TLG, such as the G mode position and width and the relative shift of the combinational mode, are also observed here (Figure 5(i)). The TEM measurements of the same TLG studied by Raman spectroscopy are presented in Figure 6. The low-magnification TEM image (Figure 6(a)) indicates that the TLG flake was transferred from the SiO_2/Si substrate to the normal TEM Cu grid without any noticeable change. The edge/crystal orientation of the TLG, identified by the Raman study, is shown in the optical image in Figure 6(b), where the TLG flake is rotated along the same direction in the TEM image for comparison. Figure 6(c) shows the HRTEM image of the ABA-stacked domain without a filter. The enlarged image (Figure 6(d))

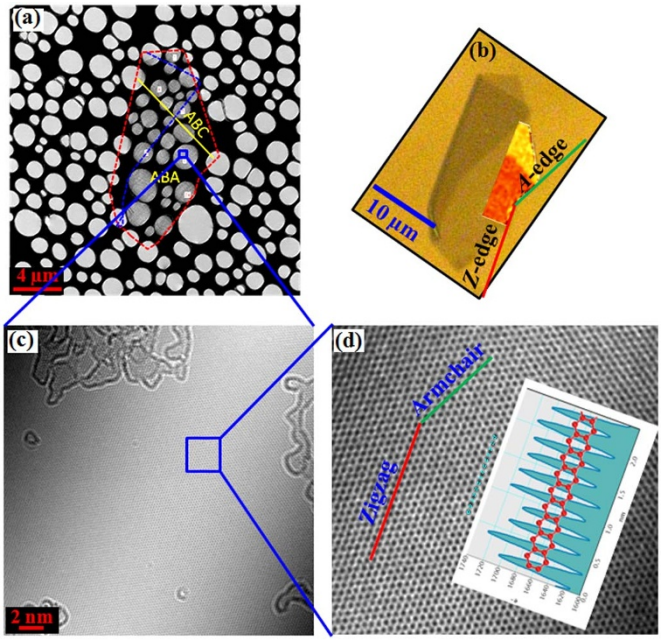

Figure 6 | (a) A TEM image of the TLG. The yellow and blue lines highlight the boundary between two domains and the folded area, respectively. (b) An optical image of the TLG. The Raman image indicates the edge/crystal orientations and stacking orders. (c) HRTEM image of the ABA-stacked domain. (d) An enlargement of the selected area in (c). The zigzag and armchair orientations are labeled by red and green lines, respectively. The inset shows the line intensity profile along the selected line as illustrated.

allows for zigzag and armchair orientation identification, which can also be identified by the FFT of the image, as in inset of Figure 4(c). The zigzag and armchair directions in the image and the line intensity profile also match our Raman measurements.

A reliable way to identify the ABA-stacked (Bernal) and ABC-stacked (rhombohedral) TLG by HRTEM is to compare their defocus-dependent patterns[27]. As shown in Figures 7(c) and 7(d), in addition to the inversion of the contrast (black to white, marked with red circles in Figures 7(c) and 7(d)), the contrast of the individual dots in ABA-stacked TLG is significantly different when the defocus value is changed. For example, it can be seen in Figure 7(d) that three dots appear to have the most intense contrast (either darkest (marked with red solid dots) or brightest (marked with green solid dots)). This is due to the strongest diffraction of the e-beam by the three overlapping carbon atoms in the three layers, in contrast to the relatively weak contrast of the dots caused by the two overlapping carbon atoms or by non-overlapping carbon atoms. In contrast to ABA-stacked TLG, there are always two overlapping carbon atoms along the *c*-axis in ABC-stacked TLG. Therefore, the contrast of the diffracted dots is uniform regardless of the focus level[27]. This is demonstrated in the HRTEM images shown in Figures 8(c) and 8(d). All the dots (marked with red and green solid dots in Figures 8(c) and 8(d), respectively) have the same intensity even though their contrast changes from white to black (marked with red circles in Figures 8(c) and 8(d)) when the defocus is varied.

Discussion

Meyer *et al.*[52] achieved a ~25% success rate by transferring graphene flakes from SiO_2/Si substrates onto a specially fabricated TEM grid. We found that treatment of the SiO_2/Si substrate by O_2 plasma increased the success rate to more than 70% even when the graphene flakes were transferred from SiO_2/Si substrates onto a normal TEM grid. This was mainly because graphene samples on the O_2 plasma-treated SiO_2/Si substrates were easier to detach from the substrate because of the enhanced hydrophilicity of the SiO_2 surfaces from O_2 plasma treatment.

Our simple yet efficient method for transferring graphene flakes onto a normal TEM grid allowed us to study the in-plane and out-of-plane arrangements of carbon atoms in BLG and TLG by both Raman spectroscopy and HRTEM. By monitoring the Raman spectral features such as the integrated intensity of the D mode, the position of the G mode and the width of the G′ mode, we could precisely identify the edge/crystal orientations and the stacking orders of BLG and TLG. HRTEM measurements of exactly the same BLG and TLG flakes allowed us to visualize the structures of individual carbon atoms and reiterated the Raman measurements. Our work has successfully demonstrated that Raman spectroscopy and HRTEM imaging can be used together to determine the edge/crystal orientations and stacking orders of graphene layers, which is useful for our further understanding of the fundamental physics of graphene layers and for developing applications based on the unique properties of graphene layers influenced by their edge/crystal orientations and stacking orders.

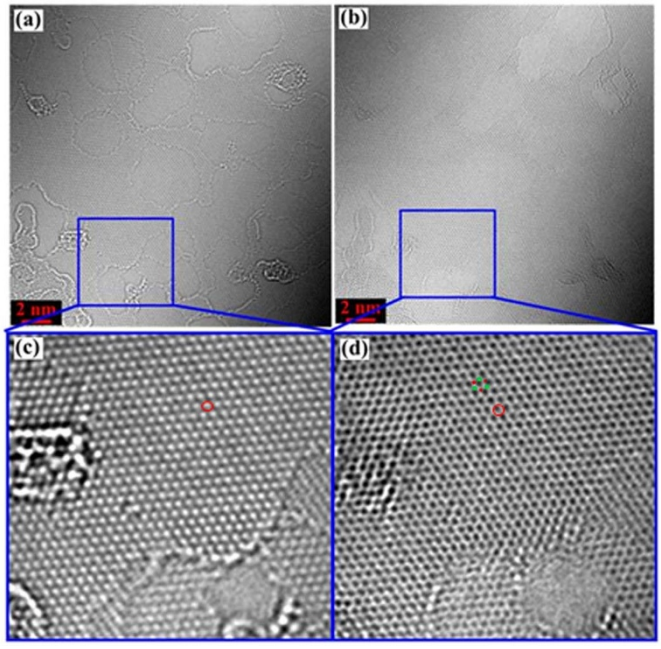

Figure 7 | (a) and (b) HRTEM images of ABA-stacked TLG taken at different defocus values. (c) and (d) High magnification images of the selected areas in (a) and (b).

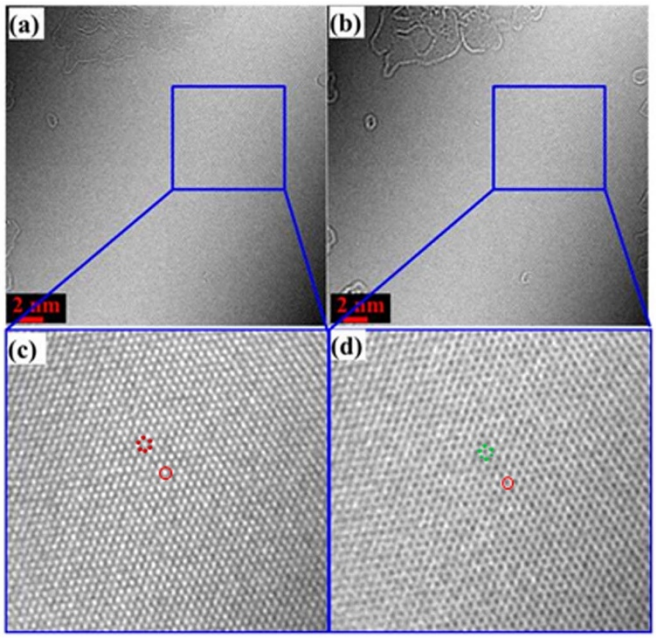

Figure 8 | (a) and (b) HRTEM images of ABC-stacked TLG taken at different defocus values. (c) and (d) High magnification images of the selected areas in (a) and (b).

Methods

In this work, graphene samples were prepared by micromechanical cleavage of natural graphite crystals or HOPG[51] and transferred on O_2 plasma-treated 300 nm SiO_2/Si substrates. The treatment of SiO_2/Si substrates by O_2 plasma was performed using March PX-250 plasma system with 100 W power and 70 mTorr base pressure. Pure oxygen gas was used as the plasma source. The targeted graphene flakes were transferred onto a normal TEM Cu grid based on the method developed by Meyer *et al.*[52] Raman spectra and images were obtained by a WITec CRM200 confocal microscopy Raman system with a piezocrystal controlled scanning stage. The excitation laser wavelength was 532 nm and its spot size was around 500 nm. To avoid damage and heating, the laser power was controlled below 2 mW. TEM measurements were carried out on an aberration-corrected and monochromated FEI Titan 60-300 microscope. The microscope was operated at 60 kV to minimize the knock-on damage to the graphene. The spherical aberration of the microscope was tuned to a negative value of about 6 μm, and the energy spread of the electron beam was reduced to below 0.2 eV from about 0.8 eV so that the information limit was better than 1.4 angstroms. The images were recorded on a charge-coupled device (CCD) camera (2 k × 2 k, Gatan UltraScan™ 1000).

1. Nakada, K., Fujita, M., Dresselhaus, G. & Dresselhaus, M. S. Edge state in graphene ribbons: Nanometer size effect and edge shape dependence. *Phys. Rev. B* **54**, 17954–17961 (1996).
2. Sasaki, K., Sato, K., Saito, R. & Jiang, J. Local density of states at zigzag edges of carbon nanotubes and graphene. *Phys. Rev. B* **75**, 235430-1–235430-7 (2007).
3. Sasaki, K., Jiang, J., Saito, R., Onari, S. & Tanaka, Y. Theory of superconductivity of carbon nanotubes and graphene. *J. Phys. Soc. Jpn.* **76**, 033702-1–033702-4 (2007).

4. Abanin, D. A., Lee, P. A. & Levitov, L. S. Charge and spin transport at the quantum Hall edge of graphene. *Solid State Commun.* **143**, 77–85 (2007).
5. Cervantes-Sodi, F., Csanyi, G., Piscanec, S. & Ferrari, A. C. Edge-functionalized and substitutionally doped graphene nanoribbons: Electronic and spin properties. *Phys. Rev. B* **77**, 165427-1–165427-13 (2008).
6. Son, Y. W., Cohen, M. L. & Louie, S. G. Half-metallic graphene nanoribbons. *Nature* **444**, 347–349 (2006).
7. Yang, L., Cohen, M. L. & Louie, S. G. Excitonic effects in the optical spectra of graphene nanoribbons. *Nano Lett.* **7**, 3112–3115 (2007).
8. Moghaddam, A. G. & Zareyan, M. Graphene-based superconducting quantum point contacts. *Appl. Phys. A-Mater.* **89**, 579–585 (2007).
9. Wang, W. L., Meng, S. & Kaxiras, E. Graphene nanoflakes with large spin. *Nano Lett.* **8**, 241–245 (2008).
10. Enoki, T., Kobayashi, Y. & Fukui, K. I. Electronic structures of graphene edges and nanographene. *Int. Rev. Phys. Chem.* **26**, 609–645 (2007).
11. Zhang, L. Y., Zhang, Y., Camacho, J., Khodas, M. & Zaliznyak, I. The experimental observation of quantum Hall effect of l = 3 chiral quasiparticles in trilayer graphene. *Nat. Phys.* **7**, 953–957 (2011).
12. Kumar, A. *et al.* Integer Quantum Hall Effect in Trilayer Graphene. *Phys. Rev. Lett.* **107**, 126806-1–126806-4 (2011).
13. Bao, W. *et al.* Stacking-dependent band gap and quantum transport in trilayer graphene. *Nat. Phys.* **7**, 948–952 (2011).
14. Koshino, M. Interlayer screening effect in graphene multilayers with ABA and ABC stacking. *Phys. Rev. B* **81**, 125304-1–125304-7 (2010).
15. Avetisyan, A. A., Partoens, B. & Peeters, F. M. Stacking order dependent electric field tuning of the band gap in graphene multilayers. *Phys. Rev. B* **81**, 115432-1–115432-7 (2010).
16. Mak, K. F., Shan, J. & Heinz, T. F. Electronic Structure of Few-Layer Graphene: Experimental Demonstration of Strong Dependence on Stacking Sequence. *Phys. Rev. Lett.* **104**, 176404-1–176404-4 (2010).
17. Zhang, F., Sahu, B., Min, H. K. & MacDonald, A. H. Band structure of ABC-stacked graphene trilayers. *Phys. Rev. B* **82**, 035409-1–035409-10 (2010).
18. Almeida, C. M., Carozo, V., Prioli, R. & Achete, C. A. Identification of graphene crystallographic orientation by atomic force microscopy. *J. Appl. Phys.* **110**, 086101-1–086101-3 (2011).
19. Neubeck, S. *et al.* Direct determination of the crystallographic orientation of graphene edges by atomic resolution imaging. *Appl. Phys. Lett.* **97**, 053110-1–053110-3 (2010).
20. Girit, C. O. *et al.* Graphene at the Edge: Stability and Dynamics. *Science* **323**, 1705–1708 (2009).
21. You, Y. M., Ni, Z. H., Yu, T. & Shen, Z. X. Edge chirality determination of graphene by Raman spectroscopy. *Appl. Phys. Lett.* **93**, 163112-1–163112-3 (2008).
22. Begliarbekov, M., Sul, O., Kalliakos, S., Yang, E. H. & Strauf, S. Determination of edge purity in bilayer graphene using μ-Raman spectroscopy. *Appl. Phys. Lett.* **97**, 031908-1–031908-3 (2010).
23. Sasaki, K., Saito, R., Wakabayashi, K. & Enoki, T. Identifying the Orientation of Edge of Graphene Using G Band Raman Spectra. *J. Phys. Soc. Jpn.* **79**, 044603-1–044603-8 (2010).
24. Cong, C. X., Yu, T. & Wang, H. M. Raman Study on the G Mode of Graphene for Determination of Edge Orientation. *ACS Nano* **4**, 3175–3180 (2010).
25. Gupta, A. K., Russin, T. J., Gutierrez, H. R. & Eklund, P. C. Probing Graphene Edges via Raman Scattering. *ACS Nano* **3**, 45–52 (2009).
26. Casiraghi, C. *et al.* Raman Spectroscopy of Graphene Edges. *Nano Lett.* **9**, 1433–1441 (2009).
27. Warner, J. H., Mukai, M. & Kirkland, A. I. Atomic Structure of ABC Rhombohedral Stacked Trilayer Graphene. *ACS Nano* **6**, 5680–5686 (2012).
28. Lui, C. H. *et al.* Imaging Stacking Order in Few-Layer Graphene. *Nano Lett.* **11**, 164–169 (2011).
29. Cong, C. X. *et al.* Raman Characterization of ABA- and ABC-Stacked Trilayer Graphene. *ACS Nano* **5**, 8760–8768 (2011).
30. Cong, C. X., Yu, T., Saito, R., Dresselhaus, G. F. & Dresselhaus, M. S. Second-Order Overtone and Combination Raman Modes of Graphene Layers in the Range of 1690–2150 cm^{-1}. *ACS Nano* **5**, 1600–1605 (2011).
31. Ferrari, A. C. *et al.* Raman spectrum of graphene and graphene layers. *Phys. Rev. Lett.* **97**, 187401-1–187401-4 (2006).
32. Ni, Z. H. *et al.* Graphene thickness determination using reflection and contrast spectroscopy. *Nano Lett.* **7**, 2758–2763 (2007).
33. Malard, L. M., Pimenta, M. A., Dresselhaus, G. & Dresselhaus, M. S. Raman spectroscopy in graphene. *Phys. Rep.* **473**, 51–87 (2009).
34. Malard, L. M., Mafra, D. L., Doorn, S. K. & Pimenta, M. A. Resonance Raman scattering in graphene: Probing phonons and electrons. *Solid State Commun.* **149**, 1136–1139 (2009).
35. Malard, L. M. *et al.* Electronic properties of bilayer graphene probed by Resonance Raman Scattering. *Phys. Status. Solidi. B* **245**, 2060–2063 (2008).
36. Yan, J., Zhang, Y. B., Kim, P. & Pinczuk, A. Electric field effect tuning of electron-phonon coupling in graphene. *Phys. Rev. Lett.* **98**, 166802-1–166802-4 (2007).
37. Yan, J., Henriksen, E. A., Kim, P. & Pinczuk, A. Observation of anomalous phonon softening in bilayer graphene. *Phys. Rev. Lett.* **101**, 136804-1–136804-4 (2008).
38. Luo, Z. Q., Cong, C. X., Zhang, J., Xiong, Q. H. & Yu, T. Direct observation of inner and outer G ' band double-resonance Raman scattering in free standing graphene. *Appl. Phys. Lett.* **100**, 243107-1–243107-4 (2012).
39. Mafra, D. L. *et al.* Determination of LA and TO phonon dispersion relations of graphene near the Dirac point by double resonance Raman scattering. *Phys. Rev. B* **76**, 233407-1–233407-4 (2007).
40. Das, A. *et al.* Monitoring dopants by Raman scattering in an electrochemically top-gated graphene transistor. *Nat. Nanotechnol.* **3**, 210–215 (2008).
41. Luo, Z. Q. *et al.* Thickness-Dependent Reversible Hydrogenation of Graphene Layers. *ACS Nano* **3**, 1781–1788 (2009).
42. Peimyoo, N., Yu, T., Shang, J. Z., Cong, C. X. & Yang, H. P. Thickness-dependent azobenzene doping in mono- and few-layer graphene. *Carbon* **50**, 201–208 (2012).
43. Cancado, L. G. *et al.* Stokes and anti-Stokes double resonance Raman scattering in two-dimensional graphite. *Phys. Rev. B* **66**, 035415-1–035415-5 (2002).
44. Cancado, L. G. *et al.* Quantifying Defects in Graphene via Raman Spectroscopy at Different Excitation Energies. *Nano Lett.* **11**, 3190–3196 (2011).
45. Yu, T. *et al.* Raman mapping investigation of graphene on transparent flexible substrate: The strain effect. *J. Phys. Chem. C* **112**, 12602–12605 (2008).
46. Huang, M. Y. *et al.* Phonon softening and crystallographic orientation of strained graphene studied by Raman spectroscopy. *P. Natl. Acad. Sci. USA* **106**, 7304–7308 (2009).
47. Mohiuddin, T. M. G. *et al.* Uniaxial strain in graphene by Raman spectroscopy: G peak splitting, Gruneisen parameters, and sample orientation. *Phys. Rev. B* **79**, 205433-1–205433-8 (2009).
48. Ni, Z. H. *et al.* Uniaxial Strain on Graphene: Raman Spectroscopy Study and Band-Gap Opening. *ACS Nano* **2**, 2301–2305 (2008).
49. Meyer, J. C. *et al.* Direct Imaging of Lattice Atoms and Topological Defects in Graphene Membranes. *Nano Lett.* **8**, 3582–3586 (2008).
50. Meyer, J. C. *et al.* Accurate Measurement of Electron Beam Induced Displacement Cross Sections for Single-Layer Graphene. *Phys. Rev. Lett.* **108** 196102-1–196102-6 (2012).
51. Novoselov, K. S. *et al.* Electric field effect in atomically thin carbon films. *Science* **306**, 666–669 (2004).
52. Meyer, J. C., Girit, C. O., Crommie, M. F. & Zettl, A. Hydrocarbon lithography on graphene membranes. *Appl. Phys. Lett.* **92**, 123110-1–123110-3 (2008).
53. Cancado, L. G., Pimenta, M. A., Neves, B. R. A., Dantas, M. S. S. & Jorio, A. Influence of the atomic structure on the Raman spectra of graphite edges. *Phys. Rev. Lett.* **93**, 247401-1–247401-4 (2004).

Acknowledgements

The work described here was supported by the Singapore National Research Foundation under Award No. NRF-RF2010-07 and MOE Tier 2 MOE2009-T2-1-037.

Author contributions

C.X.C. and T.Y. initialled the project and conceived and designed the experiments; C.X.C. T.Y. and K.L. performed the experiments; C.X.C. and T.Y. collected and analysed the data and co-wrote the paper. All authors discussed the results and commented on the manuscript.

Additional information

Supplementary information accompanies this paper at http://www.nature.com/scientificreports

Competing financial interests: The authors declare no competing financial interests.

How to cite this article: Cong, C., Li, K., Zhang, X.X. & Yu, T. Visualization of arrangements of carbon atoms in graphene layers by Raman mapping and atomic-resolution TEM. *Sci. Rep.* **3**, 1195; DOI:10.1038/srep01195 (2013).